



Plasmonic Heating-Promoted Photothermal Synthesis of α -Cyanoacrylonitriles Over Au/h-BN Catalysts

Ce Liang¹, Yuanyuan Zhang¹, Bin Zhang¹, Xin-Miao Liu¹, Guo-Lin Gao¹, Jingyan Cao^{2*} and Ping Xu^{1*}

¹MIT Key Laboratory of Critical Materials Technology for New Energy Conversion and Storage, School of Chemistry and Chemical Engineering, Harbin Institute of Technology, Harbin, China, ²Department of Medical Oncology, Harbin Medical University Cancer Hospital, Harbin, China

OPEN ACCESS

Edited by:

Van-Huy Nguyen,
Binh Duong University, Vietnam

Reviewed by:

Lan Anh Phan Thi,
Vietnam National University, Hanoi,
Vietnam
Anh Phan,
Phenikaa University, Vietnam

*Correspondence:

Ping Xu
pxu@hit.edu.cn
Jingyan Cao
caojingyan@hrbmu.edu.cn

Specialty section:

This article was submitted to
Physical Chemistry and Chemical
Physics,
a section of the journal
Frontiers in Chemistry

Received: 28 June 2021

Accepted: 23 August 2021

Published: 08 September 2021

Citation:

Liang C, Zhang Y, Zhang B, Liu X-M,
Gao G-L, Cao J and Xu P (2021)
Plasmonic Heating-Promoted
Photothermal Synthesis of
 α -Cyanoacrylonitriles Over Au/h-
BN Catalysts.
Front. Chem. 9:732162.
doi: 10.3389/fchem.2021.732162

Plasmonic nanoparticle-involved materials play an essential role in the field of photothermal conversion. Herein, we report the application of photothermal heterogeneous catalysts consisting of gold nanoparticles decorated on defect-rich h-BN sheets (Au/h-BN) for the photocatalytic synthesis of α -cyanoacrylonitriles under mild conditions. It has been demonstrated the $-NH_2$ groups present in the defect-rich h-BN act as the catalytically active sites, while plasmonic heating from the gold nanoparticles can drive the reaction by providing local heat. Au/h-BN catalyst can work for a broad substrate scope in the synthesis of α -cyanoacrylonitriles, and a plausible $-NH_2$ group-involved reaction mechanism has been proposed. This work may open up new avenues in photothermal catalysis by combining plasmonic materials and catalytic sites in one system.

Keywords: plasmonic heating, photothermal catalysis, Au/h-BN, α -cyanoacrylonitriles, reaction mechanism

INTRODUCTION

Thermal energy is one of the most commonly used energy sources in human life and production (Fan, 2017). Among various methods of obtaining thermal energy, photothermal conversion has a bright future due to its convenient, efficient, and green nature (Zhu et al., 2018). Photothermal conversion is usually accomplished by photothermal agents, which convert light energy into heat via light absorption and non-radiation processes. Particularly, plasmonic photothermal materials that rely on localized surface plasmon resonance (LSPR) exhibit remarkable advantages since the LSPR property can be easily manipulated by tuning their shape, size, composition and surrounding medium (Jauffred et al., 2019). For this reason, plasmonic photothermal materials have been broadly utilized in the areas of water recycling (Zhang et al., 2019), catalysis (Mateo et al., 2021), photothermal therapy (Cheng et al., 2014) etc. (Kim et al., 2019). Generally, LSPR generates heat to go through three processes: 1) The incident light resonates with the electron cloud of nanomaterials to generate a locally enhanced electromagnetic field (Kazuma and Kim, 2019). 2) The oscillation of free electrons rapidly decays through the formation of hot charge carriers (hot electrons and holes) (Zhang et al., 2018; Li and Jin, 2020). Notably, these hot carries can induce several reactions, such as ethylene epoxidation (Christopher et al., 2011), hydrogenation of carbonyl compounds (Landry et al., 2017), etc. (Dai et al., 2015; Yin et al., 2020). Our group also reported a number of studies on the dimerization reactions of 4-aminothiophenol or 4-nitrothiophenol to 4,4'-dimercaptoazobenzene (Kang et al., 2013; Xu et al., 2013; Kang et al.,

2015; Shen et al., 2018; Liang et al., 2020; Li et al., 2021). 3) The photoexcited hot carriers evolve to a Fermi–Dirac distribution via electron–electron scattering (Jiang et al., 2018). Then heat is generated through electron–phonon scattering and eventually releases to the surrounding medium (Jauffred et al., 2019). In fact, plasmonic heating has been successfully utilized in some chemical transformations but relatively rare (Lemieux et al., 2006; Adleman et al., 2009; Zhao et al., 2015). For example, Boyd and co-workers reported the use of plasmonic heat generated around Au nanoparticles to promote steam reforming of ethanol to form CO₂, CO and H₂ (Adleman et al., 2009). Also, the group of Branda disclosed a thermally enhanced plasmonic photocatalysis of a retro Diels–Alder reaction using Au nanoparticles (Lemieux et al., 2006). Moreover, Xiong et al. described Pd–Ag alloy nanocages for the photothermally catalyzed hydrogenation of styrene (Zhao et al., 2015).

Encouraged by these findings, herein, we demonstrate gold nanoparticles on defect-rich h-BN sheets (Au/h-BN) as a photothermal catalyst for the synthesis of α -cyanoacrylonitriles. α -Cyanoacrylonitriles have played critical roles as synthetic intermediates (Cutrí et al., 1998), riot control agents (Jones, 1972), pre-polymers (Lee et al., 2007; Kharas et al., 2009), piezoelectric materials (Lee et al., 2003), and optoelectronic devices (Aloui et al., 2016). Moreover, in drug discovery, α -cyanoacrylonitriles are potential compounds with cytostatic (Latif et al., 1970), anti-inflammatory (Girgis et al., 2007), hypotensive (El-Sadek et al., 2007), and bronchodilatory (Girgis et al., 2015) properties. Therefore, studying the synthesis of α -cyanoacrylonitriles is of great importance for future applications. In terms of Au/h-BN, the Au nanoparticles act as plasmonic nanoheaters, which generate heat upon light irradiation and then transfer the heat to the defect-rich h-BN support containing active catalytic sites. This process can drive the cyanation reaction under mild conditions, which we believe can be applied in other photothermally driven organic syntheses.

EXPERIMENTAL SECTION

Preparation of Au Nanoparticles

The Au nanoparticles were synthesized according to a reported protocol (Frens, 1973). 100 ml of HAuCl₄ solution (10⁻² wt% in water) was added into a 250 ml three-necked round-bottomed flask and then heated with a heating mantle for 15 min under vigorous stirring. A condenser was utilized to prevent the evaporation of the solvent. After boiling (100°C) had commenced, 0.32 ml of sodium citrate (1 wt% in water) was injected. The color of the solution changed from yellow to bluish-gray and then to purplish-red in 30 min, indicating the formation of gold nanoparticles.

Preparation of Defect-Rich h-BN

The defect-rich h-BN sheets were prepared as reported with some modifications (Feng et al., 2019). 5 g urea and 1 g boric acid were dissolved in 10 ml deionized water to form a homogeneous solution, which was heated to 80°C for recrystallization. A white crystalline powder was obtained upon evaporation of the

solvent, which was then put into a horizontal tube furnace. After removal the air with nitrogen, the furnace was heated up to 800°C at a heating rate of 5°C/min and the powder was annealed at 800°C for 2 h under the protection of nitrogen. After that, pyrolysis product was obtained and washed with hot water to remove boron oxide and obtain defect-rich h-BN.

Preparation of Au/h-BN Nanocatalysts

50 mg defect-rich h-BN was added into a 50 ml Au dispersion (0.1 mg/ml in water) and stirred for 24 h at room temperature. The resulting dispersed solution was filtered with a 0.1 μ m pore size membrane to separate the unattached Au nanoparticles from the Au/h-BN nanocomposite.

Characterization

X-ray diffraction (XRD) patterns were collected on a Rigaku D/MAXRC X-ray diffractometer (45.0 kV, 50.0 mA) ray diffractometer with Cu K α radiation (λ = 0.15406 nm). Transmission electron microscopic (TEM) images were taken by an FEI Tecnai F20 operating at an accelerating voltage of 200 kV. The Fourier transform infrared (FT-IR) spectra were obtained on a Thermo Scientific Nicolet iS5 FT-IR spectrometer. X-ray photoelectron spectra (XPS) were recorded on a PHI-5700 ESCA system using Al K α radiation as a source ($h\nu$ = 1,486.6 eV) and binding energy values were reported relative to the C 1s of surface adsorbed carbon (= 284.5 eV). UV-visible absorption spectra were analyzed were gained on a Persee TU-1901 spectrophotometer. Photothermal images were measured by a Fotric 225s infrared camera while illuminating the sample (2 mg h-BN and 2 mg Au/h-BN dispersed in 1 ml acetonitrile, respectively) with a 300 W Xe lamp (PLS-SXE300/300UV, wavelength: 330–2,500 nm, beam diameter: 30 mm). Flash column chromatography was performed using 200–300 mesh silica gel. All materials and solvents were used as received from commercial sources without further purification unless otherwise noted. ¹H and ¹³C NMR spectra were obtained on a Bruker AV-400 or AV-600 instrument in CDCl₃ or DMSO-d₆ with TMS (SiMe₄) as an internal standard, and chemical shift values were reported in ppm relative to dimethyl TMS (δ = 0.00 ppm) or DMSO (δ = 2.50 ppm) for ¹H NMR, chloroform (δ = 77.0 ppm), or DMSO (δ = 39.5 ppm) for ¹³C NMR. The reported chemical shifts (δ) of ¹³C NMR were ¹³C{¹H} proton-decoupled carbons data. The following abbreviations (or combinations thereof) were used to explain multiplicities: s = singlet, d = doublet, t = triplet, q = quartet, and m = multiplet.

Computational Methods

All geometric optimization and energy analysis were performed utilizing the Gaussian09 software package. The DFT calculations were conducted using the B3LYP exchange–correlation functional. The 6-31G(d, p) basis set was chosen for C, H, O, B and N atoms. The model of the catalyst was simulated with 19 B atoms, 20 N atoms and 17 H atoms, where B and N atoms were alternately connected along with an amino group hanging on the edge. Adding hydrogen atoms at the end can avoid the unsaturated boundary effect. To facilitate the calculations of free energy change in the reactions, Au nanoparticles were

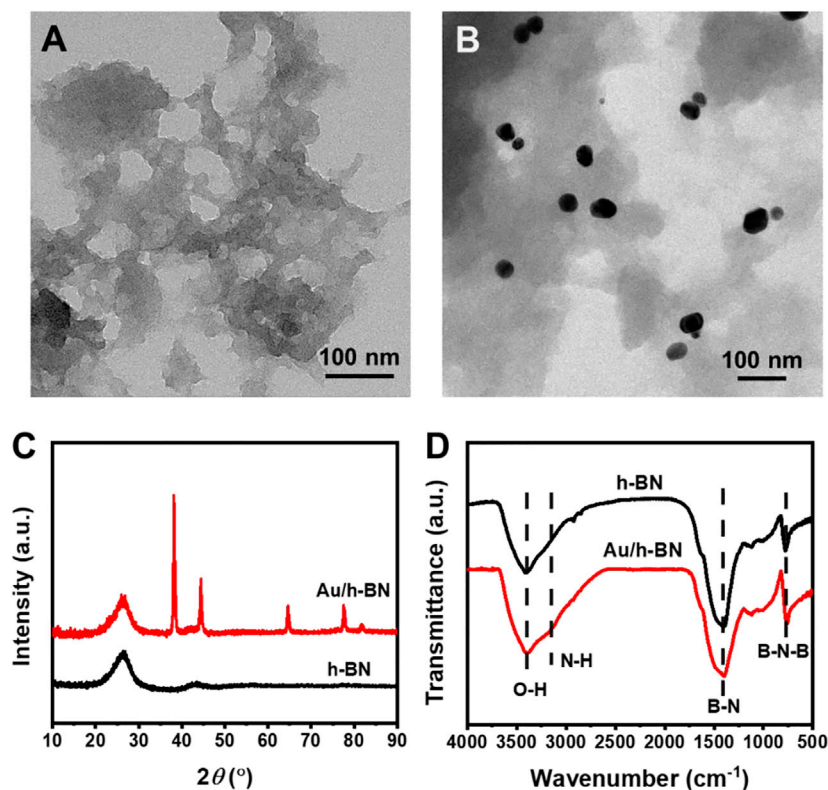


FIGURE 1 | TEM images for (A) bare h-BN and (B) Au/h-BN composite. (C) XRD patterns and (D) FTIR spectra for Au/h-BN composite and bare h-BN.

omitted during the calculations because the experimental results showed that the Au nanoparticles only act as nanoheaters instead of catalytic sites.

Photothermal Reaction Conditions

In a 10 ml vial, aldehydes (0.10 mmol), malononitrile (0.13 mmol), Au/h-BN (2.0 mg), and anhydrous MeCN (1.0 ml) were added in sequence under magnetic stirring, and then the vial was sealed. The system was evacuated by five freeze pump-thaw cycles and back-filled with N_2 . Then, the vial was irradiated by a Xe lamp for 18 h. After reaction completion, the vial contents were evaporated under reduced pressure. The residue was purified by precipitation thin-layer chromatography (PTLC) using PE/EtOAc (60:1 to 1:1 depending on the substrates) as the eluent to afford the desired product.

RESULTS AND DISCUSSION

Synthesis and Characterization of Au/h-BN

Au/h-BN nanocatalysts were produced through a wet-impregnation strategy (see detail in Experimental Section). In brief, Au nanoparticles and defect-rich h-BN were first prepared separately and then combined to form the Au/h-BN composites. TEM was carried out to reveal the transparent nanosheet morphology of the synthesized h-BN, as shown in **Figure 1A**. Additionally, many pores are observed, which can serve as

nanoreactors and thus are beneficial for heterogeneous catalysis. This porous structure implies that the synthesized h-BN is defect-rich because an ideal perfect h-BN is a flawless two-dimensional matrix. Furthermore, **Supplementary Figure S1** in supporting information showed the morphology of Au nanoparticles was nanospheres with an average diameter of ~ 30 nm. Notably, **Figure 1B** reveals that the h-BN surface is successfully decorated with Au nanoparticles, indicating the formation of Au/h-BN composite as expected. These results were supported by powder XRD patterns (**Figure 1C**). Two broad peaks at 26.6° and 43.5° can be indexed to h-BN (PDF#85-1068). The broad feature suggests its low crystallinity. Furthermore, the peaks at 38.2° , 44.4° , 64.6° , 77.5° and 81.7° in the Au/h-BN composite are from gold (PDF#89-3697). Fourier-transform infrared spectroscopy was carried out to investigate the chemical structures of samples (**Figure 1D**). The absorption peaks at $1,390$ and 778 cm^{-1} are attributed to the in-plane B-N stretching vibration and the out-of-plane B-N-B bending bands, respectively (Weng et al., 2015). In addition, the bands at $3,180$ and $3,400\text{ cm}^{-1}$ indicate the presence of amino and hydroxyl functional groups (Ou et al., 2017). This confirms that B and N atoms are not entirely cross-linked to form a perfect two-dimensional structure. In other words, the amino and hydroxyl groups are present as dangling bonds at the edge or pores of the defect-rich h-BN.

The XPS spectra were also collected to study the bonding state of the Au/h-BN composite (**Figures 2A–D**). In the N 1s spectrum (**Figure 2B**), the main component centered at 398.1 eV

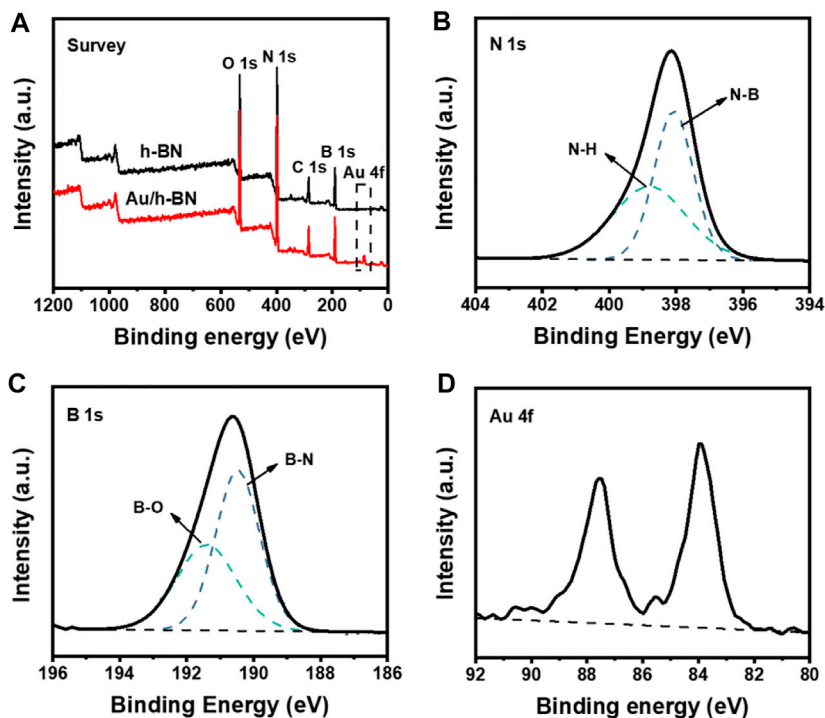


FIGURE 2 | (A) XPS survey spectra for Au/h-BN composite and bare h-BN. (B) N 1s (C) B 1s and (D) Au 4f spectra for Au/h-BN composite.

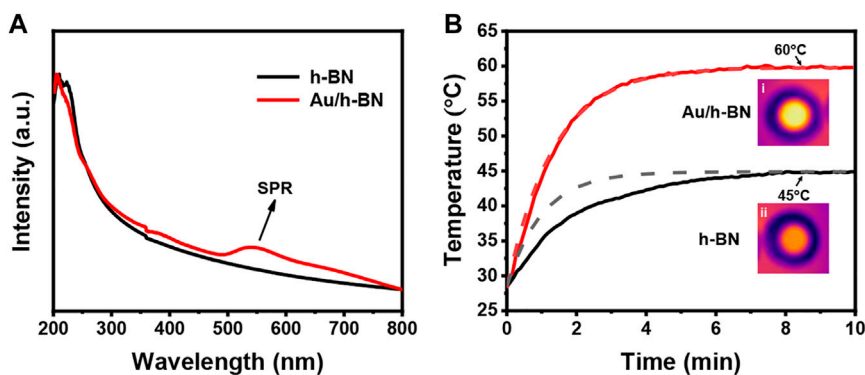
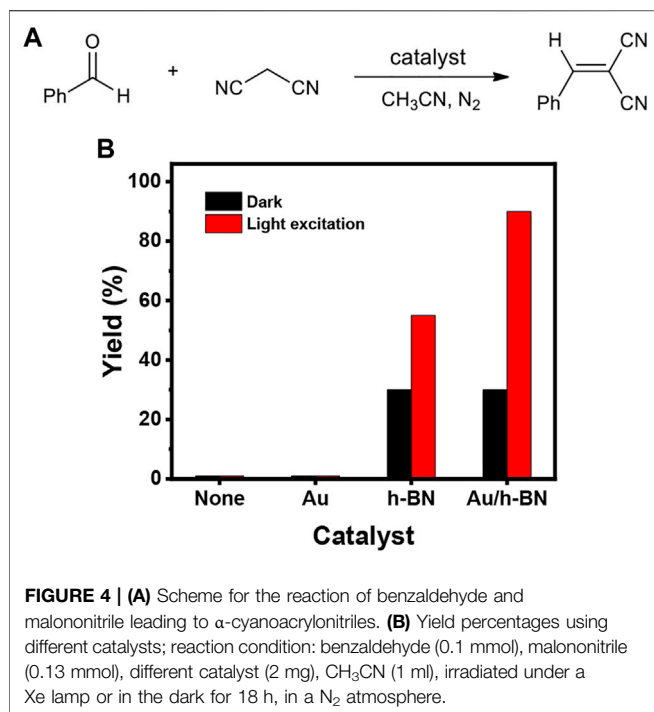


FIGURE 3 | (A) UV-vis spectra for Au/h-BN composite and bare h-BN. (B) Temperature-time curves for Au/h-BN suspension and h-BN suspension. Solid curves and dash lines correspond to the experimental data and theoretical calculations, respectively. The insets are experimental IR thermal images from top views.

corresponded to the N-B band, whereas the higher binding energy at 398.8 eV was caused by amino groups (Zhi et al., 2009). The B 1s spectrum was depicted in **Figure 2C**, and the dominant peak at 190.5 eV accounts for B-N bonds, and the shoulder peak at 191.4 eV is due to B-O bonds (Zhi et al., 2009; Perez et al., 2014; Liu et al., 2017). Besides the peaks of B and N, the signal of Au could be clearly observed from the Au/h-BN composite as compared to the bare h-BN (**Figures 2A,D**).

UV-vis spectroscopy was performed to measure the LSPR. As shown in **Figure 3A**, the LSPR band is centered at 545 nm for Au/h-BN composite, while bare h-BN shows no LSPR features in the

visible region. The photothermal property of the samples is the key in this study, which was disclosed by an infrared camera while illuminating the sample solution with a Xe lamp. **Figure 3B** depicts the temperature-time curves for h-BN and Au/h-BN suspension, and the insets are corresponding IR thermal images after equilibrium (from top views). Under the light irradiation, the temperature of h-BN suspension can reach 45°C, due to light excited and coupled phonons in the lattices (Lopez et al., 2018). Notably, a higher temperature can be obtained on the Au/h-BN composite, an increase of 15°C–60°C due to the plasmonic heating from Au. This temperature is high



Photothermal Catalytic Properties of Au/h-BN

After ensuring the photothermal effect, the Au/h-BN catalyst was tested for cyanation reactions to establish the catalytic activity. The investigation was carried out by using benzaldehyde as a substrate (0.1 mmol, 10.6 mg, 1 equiv) and malononitrile as a cyanation reagent (0.13 mmol, 8.6 mg, 1.3 equiv) with or without different catalysts (2 mg, 18.8 wt%) in 1 ml CH_3CN under a N_2 atmosphere in the dark or under light excitation (Figure 4). When the reaction was performed without catalyst, only trace product was detected after 18 h either in dark or under light irradiation, implying a catalyst for this reaction is required. A similar yield was observed when Au nanoparticles were used as a catalyst, indicating Au (and hot electrons) do not catalyze the reaction under the employed conditions. For the h-BN and Au/h-BN catalysts, the desired product was obtained in the dark in 31 and 30% yields, respectively. This catalytic activity results from the active sites at the hanging bond of the defective h-BN, as discussed above. Under light irradiation, only a limited increase in the product yield is observed for the bare h-BN (from 31 to 55%). In contrast, a remarkable increase is achieved for the Au/h-BN composite (from 30 to 90%), attributed to the plasmonic heating effect from Au, in line with the photothermal results (Figure 3). It is also confirmed that both catalytic h-BN and the light-induced heat are crucial for the high yield of the reaction.

enough to initiate several reactions. The experimental data was fitted with a well-known theoretical function of temperature rise in photothermal effects (Duong et al., 2018; Phan et al., 2018; Phan et al., 2019): $T(t) = T_0 + A/B(1 - \exp(-Bt))$. The B was calculated by plotting $\ln(T - T_0)/(T_{\text{max}} - T_0)$ vs. time and the A was determined by $T_{\text{max}} = T_0 + A/B$. For h-BN, $A_1 = 16.21$, $B_1 = 0.98$, it can be found that the deviation between the theoretical curve and experimental values is small. For Au/h-BN, $A_2 = 23.60$, $B_2 = 0.75$, the fitted curve shows a good agreement with the experimental result.

Proposed Reaction Mechanism

On the basis of the above results and previous literature (Motokura et al., 2008; Zhang et al., 2016; Lei et al., 2018; Cao et al., 2019; Zhang et al., 2020), a plausible mechanism based on a weak base-catalyzed cycle for this reaction is proposed in Figure 5, applying the $-\text{NH}_2$ groups as catalytic sites and light-induced heat as the driving force. Firstly, an $-\text{NH}_2$ group of the catalyst abstracted a proton from malononitrile **A** to generate a carbanion **B**. Then, **B** nucleophilically attacked

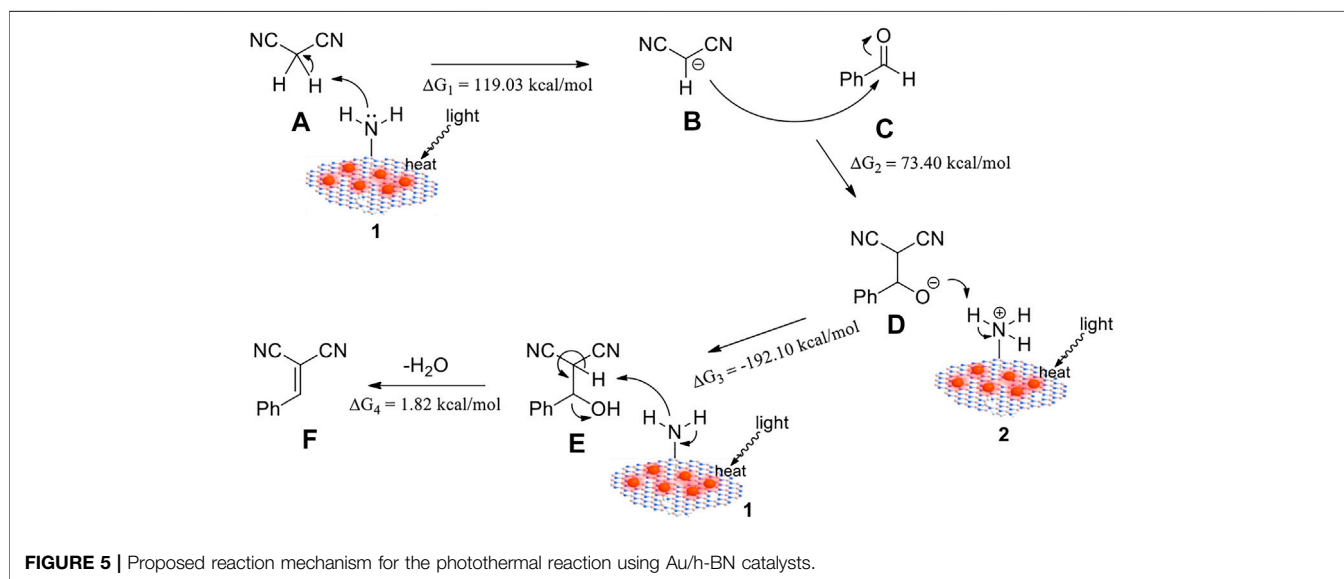


TABLE 1 | Scope of substrates for the photothermal reaction.^a

Entry	Substrate	Product	Yield (%) ^b
1			90
2			91
3			95
4			43
5			36
6			93
7			93
8			85

^aReaction condition: aldehydes (0.1 mmol), malononitrile (0.13 mmol), Au/h-BN catalyst (2 mg), CH₃CN (1 ml), irradiated under a Xe lamp for 18 h, in a N₂ atmosphere.

^bIsolated yield.

benzaldehyde **C** to form an intermediate **D**, which further reacted with the protonated catalyst, leading to an intermediate **E**. Finally, **E** eliminated a molecule of H₂O with the help of catalyst to afford the final product **F**. DFT calculations were performed to illuminate the free energy change in the reaction process. As shown in **Figure 5** and **Supplementary Figure S6**, the free energy change values $\Delta G_1 = 119.03$ kcal/mol, $\Delta G_2 = -73.40$ kcal/mol, and $\Delta G_4 = 1.82$ kcal/mol implied the endothermic steps. Also, the total free energy change $\Delta G_{\text{total}} = 2.15$ kcal/mol suggested the total reaction of benzaldehyde and malononitrile leading to α -benzylidenemalononitrile and water was endothermic. The plasmonic heating can provide energy for these processes and thus promote the reaction.

Generality of the Photothermal Reaction

The generality of the present photothermal protocol was examined. As depicted in **Table 1**, for all of the substituted aldehydes investigated, desired products were obtained in good yields (Entries 1–8). All of the α -cyanoacrylonitriles products were fully confirmed with ¹H and ¹³C NMR spectra (see **Conclusion** in **Supplementary Material** for detail). Furthermore, it is found that the substrates with an electron-donating group such as -CH₃ or -OCH₃ (**Table 1**, Entries 2 and 3)

can give higher yields than those with an electron-withdrawing group like -Cl (**Table 1**, Entries 4 and 5). Notably, the *ortho*-position (2-Cl)-substituted substrates do not hinder the reaction to form the final products in middle yields (**Table 1**, Entry 5). Moreover, furfural and substituted-furfurals are also compatible in this reaction as well, leading to the corresponding products in high yields (**Table 1**, Entry 6–8).

CONCLUSION

In summary, we have demonstrated the Au/h-BN nanocomposite as a promising photothermal catalyst for the synthesis of α -cyanoacrylonitriles. The Au/h-BN composite coupling the plasmonic heating of Au with the catalytic sites of defect-rich h-BN exhibits great catalytic activity in synthesizing α -cyanoacrylonitriles with a broad scope of substrates under mild conditions. As compared to the dark condition, the yield of the cyanation reactions can be greatly enhanced on Au/h-BN composite under light irradiation, which manifests the importance of plasmonic heating. Further development of new photothermal catalysis is under investigation in our lab.

DATA AVAILABILITY STATEMENT

The original contributions presented in the study are included in the article/**Supplementary Material**, further inquiries can be directed to the corresponding authors.

AUTHOR CONTRIBUTIONS

All authors listed have made a substantial, direct, and intellectual contribution to the work and approved it for publication.

REFERENCES

- Adleman, J. R., Boyd, D. A., Goodwin, D. G., and Psaltis, D. (2009). Heterogeneous Catalysis Mediated by Plasmon Heating. *Nano Lett.* 9, 4417–4423. doi:10.1021/nl902711n
- Aloui, W., Dhahri, N., Bouazizi, A., Boubaker, T., and Goumont, R. (2016). Optical and Electrical Properties of P-Substituted-Benzylidenemalononitrile Thin Films: Optoelectronic Applications. *Superlattices Microstruct.* 91, 302–305. doi:10.1016/j.spmi.2016.01.030
- Cao, C.-C., Chen, C.-X., Wei, Z.-W., Qiu, Q.-F., Zhu, N.-X., Xiong, Y.-Y., et al. (2019). Catalysis through Dynamic Spacer Installation of Multivariate Functionalities in Metal-Organic Frameworks. *J. Am. Chem. Soc.* 141, 2589–2593. doi:10.1021/jacs.8b12372
- Cheng, L., Wang, C., Feng, L., Yang, K., and Liu, Z. (2014). Functional Nanomaterials for Phototherapies of Cancer. *Chem. Rev.* 114, 10869–10939. doi:10.1021/cr400532z
- Christopher, P., Xin, H., and Linic, S. (2011). Visible-light-enhanced Catalytic Oxidation Reactions on Plasmonic Silver Nanostructures. *Nat. Chem.* 3, 467–472. doi:10.1038/nchem.1032
- Cutri, C. C. C., Garozzo, A., Siracusa, M. A., Sarvá, M. C., Tempera, G., Geremia, E., et al. (1998). Synthesis and Antiviral Activity of a New Series of 4-isothiazolecarbonitriles. *Bioorg. Med. Chem.* 6, 2271–2280. doi:10.1016/s0968-0896(98)80007-2
- Dai, Z.-g., Xiao, X.-h., Wu, W., Zhang, Y.-p., Liao, L., Guo, S.-s., et al. (2015). Plasmon-driven Reaction Controlled by the Number of Graphene Layers and Localized Surface Plasmon Distribution during Optical Excitation. *Light Sci. Appl.* 4, e342. doi:10.1038/lsa.2015.115
- Duong, V. T. T., Phan, A. D., Lien, N. T. H., Hue, D. T., Hoa, D. Q., Nga, D. T., et al. (2018). Near-infrared Photothermal Response of Plasmonic Gold-Coated Nanoparticles in Tissues. *Phys. Status Solidi A* 215, 1700564. doi:10.1002/pssa.201700564
- El-Sadek, M. E., Aboukull, M., El-Sabbagh, O. I., and Shallal, H. M. (2007). Synthesis of Hexahydro-1h-Pyrido[3,2-C]azepines as Hypotensive Agents of Expected Calcium-Channel Blocking Activity. *Monatsh. Chem.* 138, 219–225. doi:10.1007/s00706-007-0586-5
- Fan, S. (2017). Thermal Photonics and Energy Applications. *Joule* 1, 264–273. doi:10.1016/j.joule.2017.07.012
- Feng, C., Tang, L., Deng, Y., Zeng, G., Wang, J., Liu, Y., et al. (2019). Enhancing Optical Absorption and Charge Transfer: Synthesis of S-Doped h-BN with Tunable Band Structures for Metal-free Visible-Light-Driven Photocatalysis. *Appl. Catal. B: Environ.* 256, 117827. doi:10.1016/j.apcatb.2019.117827
- Frens, G. (1973). Controlled Nucleation for the Regulation of the Particle Size in Monodisperse Gold Suspensions. *Nat. Phys. Sci.* 241, 20–22. doi:10.1038/physci241020a0
- Girgis, A. S., Mishriky, N., Ellithy, M., Hosni, H. M., and Farag, H. (2007). Novel Synthesis of [1]-Benzothiepio[5,4-B]pyridine-3-Carbonitriles and Their Anti-inflammatory Properties. *Bioorg. Med. Chem.* 15, 2403–2413. doi:10.1016/j.bmc.2007.01.015
- Girgis, A. S., Saleh, D. O., George, R. F., Srour, A. M., Pillai, G. G., Panda, C. S., et al. (2015). Synthesis, Bioassay, and Qsar Study of Bronchodilatory Active 4h-Pyrano[3,2-C]pyridine-3-Carbonitriles. *Eur. J. Med. Chem.* 89, 835–843. doi:10.1016/j.ejmech.2013.12.032
- Jauffred, L., Samadi, A., Klingberg, H., Bendix, P. M., and Oddershede, L. B. (2019). Plasmonic Heating of Nanostructures. *Chem. Rev.* 119, 8087–8130. doi:10.1021/acs.chemrev.8b00738
- Jiang, N., Zhuo, X., and Wang, J. (2018). Active Plasmonics: Principles, Structures, and Applications. *Chem. Rev.* 118, 3054–3099. doi:10.1021/acs.chemrev.7b00252
- Jones, G. R. N. (1972). CS and its Chemical Relatives. *Nature* 235, 257–261. doi:10.1038/235257a0
- Kang, L., Han, X., Chu, J., Xiong, J., He, X., Wang, H. L., et al. (2015). *In Situ* Surface-Enhanced Raman Spectroscopy Study of Plasmon-Driven Catalytic Reactions of 4-Nitrothiophenol under a Controlled Atmosphere. *ChemCatChem* 7, 1004–1010. doi:10.1002/cctc.201403032
- Kang, L., Xu, P., Zhang, B., Tsai, H., Han, X., and Wang, H.-L. (2013). Laser Wavelength- and Power-dependent Plasmon-Driven Chemical Reactions Monitored Using Single Particle Surface Enhanced Raman Spectroscopy. *Chem. Commun.* 49, 3389–3391. doi:10.1039/c3cc40732b
- Kazuma, E., and Kim, Y. (2019). Mechanistic Studies of Plasmon Chemistry on Metal Catalysts. *Angew. Chem. Int. Ed.* 58, 4800–4808. doi:10.1002/anie.201811234
- Kharas, G. B., Hanawa, E., Hill, B. L., Atlas, S., and Raihane, M. (2009). Novel Copolymers of 2-Phenyl-1,1-Dicyanoethylene with 4-fluoro- and Pentafluorostyrene. *J. Macromolecular Sci. A* 46, 650–655. doi:10.1080/10601320902938665
- Kim, M., Lee, J. H., and Nam, J. M. (2019). Plasmonic Photothermal Nanoparticles for Biomedical Applications. *Adv. Sci.* 6, 1900471. doi:10.1002/adv.201900471
- Landry, M. J., Gellé, A., Meng, B. Y., Barrett, C. J., and Moores, A. (2017). Surface-plasmon-mediated Hydrogenation of Carbonyls Catalyzed by Silver Nanocubes under Visible Light. *ACS Catal.* 7, 6128–6133. doi:10.1021/acscatal.7b02128
- Latif, N., Girgis, N. S., and Michael, F. (1970). Dicyanovinyl- and Dicyanoalkyl-Dihydro-Furobenzodioxins and Analogous Substances of Potential Cytostatic Activity. *Tetrahedron* 26, 5765–5772. doi:10.1016/0040-4020(70)80014-x
- Lee, J.-Y., Bang, H.-B., and Choe, S. J. (2003). Synthesis and Properties of Novel Poly(meth)-Acrylates Containing Tricyanocyclopropyl Groups for Piezoelectric Applications. *Polym. Int.* 52, 1428–1433. doi:10.1002/pi.1268
- Lee, J.-Y., Kim, J.-H., Jung, W.-T., and Park, Y. K. (2007). Synthesis and Nonlinear Optical Properties of Novel Y-type Polyurethanes with High thermal Stability of Dipole Alignment. *J. Mater. Sci.* 42, 3936–3943. doi:10.1007/s10853-006-0424-x
- Lei, Z., Deng, Y., and Wang, C. (2018). Multiphase Surface Growth of Hydrophobic ZIF-8 on Melamine Sponge for Excellent Oil/water Separation and Effective Catalysis in a Knoevenagel Reaction. *J. Mater. Chem. A* 6, 3258–3263. doi:10.1039/c7ta10566e
- Lemieux, V., Gauthier, S., and Branda, N. R. (2006). Selective and Sequential Photorelease Using Molecular Switches. *Angew. Chem. Int. Ed.* 45, 6820–6824. doi:10.1002/anie.200601584
- Li, C., and Jin, Y. (2020). Shell-Isolated Plasmonic Nanostructures for Biosensing, Catalysis, and Advanced Nanoelectronics. *Adv. Funct. Mater.* 31, 2008031. doi:10.1002/adfm.202008031
- Li, S., Miao, P., Zhang, Y., Wu, J., Zhang, B., Du, Y., et al. (2021). Recent Advances in Plasmonic Nanostructures for Enhanced Photocatalysis and Electrocatalysis. *Adv. Mater.* 33, 2000086. doi:10.1002/adma.202000086
- Liang, C., Lu, Z.-A., Wu, J., Chen, M.-X., Zhang, Y., Zhang, B., et al. (2020). Recent Advances in Plasmon-Promoted Organic Transformations Using Silver-Based Catalysts. *ACS Appl. Mater. Inter.* 12, 54266–54284. doi:10.1021/acsami.0c15192
- Liu, G., Meng, X., Zhang, H., Zhao, G., Pang, H., Wang, T., et al. (2017). Elemental boron for Efficient Carbon Dioxide Reduction under Light Irradiation. *Angew. Chem. Int. Ed.* 56, 5570–5574. doi:10.1002/anie.201701370
- López, J. J., Ambrosio, A., Dai, S., Huynh, C., Bell, D. C., Lin, X., et al. (2018). Large Photothermal Effect in Sub-40 Nm h-BN Nanostructures Patterned via High-Resolution Ion Beam. *Small* 14, 1800072. doi:10.1002/smll.201800072
- Mateo, D., Cerrillo, J. L., Durini, S., and Gascon, J. (2021). Fundamentals and Applications of Photo-thermal Catalysis. *Chem. Soc. Rev.* 50, 2173–2210. doi:10.1039/d0cs00357c

FUNDING

This work was supported by the National Natural Science Foundation of China (Nos. 21671047, 21871065, and 22071038).

SUPPLEMENTARY MATERIAL

The Supplementary Material for this article can be found online at: <https://www.frontiersin.org/articles/10.3389/fchem.2021.732162/full#supplementary-material>

- Motokura, K., Tada, M., and Iwasawa, Y. (2008). Cooperative Catalysis of Primary and Tertiary Amines Immobilized on Oxide Surfaces for One-Pot C-C Bond Forming Reactions. *Angew. Chem. Int. Edition* 47, 9230–9235. doi:10.1002/anie.200802515
- Ou, H., Yang, P., Lin, L., Anpo, M., and Wang, X. (2017). Carbon Nitride Aerogels for the Photoredox Conversion of Water. *Angew. Chem. Int. Ed.* 56, 10905–10910. doi:10.1002/anie.201705926
- Perez, J. P. L., McMahon, B. W., Yu, J., Schneider, S., Boatz, J. A., Hawkins, T. W., et al. (2014). Boron Nanoparticles with High Hydrogen Loading: Mechanism for B-H Binding and Potential for Improved Combustibility and Specific Impulse. *ACS Appl. Mater. Inter.* 6, 8513–8525. doi:10.1021/am501384m
- Phan, A. D., Le, N. B., Lien, N. T. H., and Wakabayashi, K. (2018). Multilayered Plasmonic Nanostructures for Solar Energy Harvesting. *J. Phys. Chem. C* 122, 19801–19806. doi:10.1021/acs.jpcc.8b05769
- Phan, A. D., Le, N. B., Nghiem, T. H. L., Woods, L. M., Ishii, S., and Wakabayashi, K. (2019). Confinement Effects on the Solar thermal Heating Process of Tin Nanoparticle Solutions. *Phys. Chem. Chem. Phys.* 21, 19915–19920. doi:10.1039/c9cp03571k
- Shen, Y., Miao, P., Hu, C., Wu, J., Gao, M., and Xu, P. (2018). SERS-based Plasmon-Driven Reaction and Molecule Detection on a Single Ag@MoS₂ Microsphere: Effect of Thickness and Crystallinity of MoS₂. *ChemCatChem* 10, 3520–3525. doi:10.1002/cctc.201800482
- Weng, Q., Ide, Y., Wang, X., Wang, X., Zhang, C., Jiang, X., et al. (2015). Design of BN Porous Sheets with Richly Exposed (002) Plane Edges and Their Application as TiO₂ Visible Light Sensitizer. *Nano Energy* 16, 19–27. doi:10.1016/j.nanoen.2015.06.004
- Xu, P., Kang, L., Mack, N. H., Schanze, K. S., Han, X., and Wang, H.-L. (2013). Mechanistic Understanding of Surface Plasmon Assisted Catalysis on a Single Particle: Cyclic Redox of 4-aminophenol. *Sci. Rep.* 3, 2997. doi:10.1038/srep02997
- Yin, H., Zheng, L.-Q., Fang, W., Lai, Y.-H., Porenta, N., Goubert, G., et al. (2020). Nanometre-scale Spectroscopic Visualization of Catalytic Sites during a Hydrogenation Reaction on a Pd/Au Bimetallic Catalyst. *Nat. Catal.* 3, 834–842. doi:10.1038/s41929-020-00511-y
- Zhang, C., Liang, H. Q., Xu, Z. K., and Wang, Z. (2019). Harnessing Solar-Driven Photothermal Effect toward the Water-Energy Nexus. *Adv. Sci.* 6, 1900883. doi:10.1002/advs.201900883
- Zhang, L., Wang, H., Shen, W., Qin, Z., Wang, J., and Fan, W. (2016). Controlled Synthesis of Graphitic Carbon Nitride and its Catalytic Properties in Knoevenagel Condensations. *J. Catal.* 344, 293–302. doi:10.1016/j.jcat.2016.09.023
- Zhang, Y., He, S., Guo, W., Hu, Y., Huang, J., Mulcahy, J. R., et al. (2018). Surface-plasmon-driven Hot Electron Photochemistry. *Chem. Rev.* 118, 2927–2954. doi:10.1021/acs.chemrev.7b00430
- Zhang, Z., Nie, X., Wang, F., Chen, G., Huang, W.-Q., Xia, L., et al. (2020). Rhodanine-based Knoevenagel Reaction and Ring-Opening Polymerization for Efficiently Constructing Multicyclic Polymers. *Nat. Commun.* 11, 3654. doi:10.1038/s41467-020-17474-0
- Zhao, X., Long, R., Liu, D., Luo, B., and Xiong, Y. (2015). Pd-Ag alloy Nanocages: Integration of Ag Plasmonic Properties with Pd Active Sites for Light-Driven Catalytic Hydrogenation. *J. Mater. Chem. A* 3, 9390–9394. doi:10.1039/c5ta00777a
- Zhi, C. Y., Bando, Y., Terao, T., Tang, C. C., Kuwahara, H., and Golberg, D. (2009). Chemically Activated boron Nitride Nanotubes. *Chem. Asian J.* 4, 1536–1540. doi:10.1002/asia.200900158
- Zhu, L., Gao, M., Peh, C. K. N., and Ho, G. W. (2018). Solar-driven Photothermal Nanostructured Materials Designs and Prerequisites for Evaporation and Catalysis Applications. *Mater. Horiz.* 5, 323–343. doi:10.1039/c7mh01064h

Conflict of Interest: The authors declare that the research was conducted in the absence of any commercial or financial relationships that could be construed as a potential conflict of interest.

Publisher's Note: All claims expressed in this article are solely those of the authors and do not necessarily represent those of their affiliated organizations, or those of the publisher, the editors and the reviewers. Any product that may be evaluated in this article, or claim that may be made by its manufacturer, is not guaranteed or endorsed by the publisher.

Copyright © 2021 Liang, Zhang, Zhang, Liu, Gao, Cao and Xu. This is an open-access article distributed under the terms of the Creative Commons Attribution License (CC BY). The use, distribution or reproduction in other forums is permitted, provided the original author(s) and the copyright owner(s) are credited and that the original publication in this journal is cited, in accordance with accepted academic practice. No use, distribution or reproduction is permitted which does not comply with these terms.